Cell Reports, Volume *22*

Supplemental Information

Dissonant Representations of Visual Space in Prefrontal Cortex during Eye Movements

Xiaomo Chen, Marc Zirnsak, and Tirin Moore

General Surgical and Electrophysiological Procedures

Each animal was surgically implanted with a titanium head post, a scleral search coil, and a cylindrical titanium recording chamber (20 mm diameter) overlaying the arcuate sulcus. A craniotomy was performed on each animal, allowing access to the FEF. All surgeries were conducted using aseptic techniques under general anaesthesia (isoflurane), and analgesics were provided during post-surgical recovery.

Electrodes were lowered into the cortex using a hydraulic microdrive (Narishige International). Activity was recorded extracellularly using linear array electrodes (U-Probe, Plexon) with 16 contacts spaced 150 mm apart. Neural activity was measured against a local reference (e.g., Britten et al., 1993; Hikosaka and Watanabe, 2000), a stainless steel guide tube, which carried the electrode array and which was positioned above the dura. At the preamplifier stage, signals were processed with 0.5 Hz 1-pole high-pass and 8kHz 4-pole low-pass anti-aliasing Bessel filters, and then divided into two streams for the recording of LFPs and spiking activity. The stream used for LFP recording was amplified (×500~2000 gain), processed by a 4-pole 200Hz low-pass Bessel filter and sampled at 1000 Hz. The stream used for spike detection was processed by a 4-pole Bessel high-pass filter (300 Hz) a 2-pole Bessel low-passed filter (6000 Hz), and was sampled at 40 kHz. No other filters were used in the analyses.

The FEF was identified by the ability to evoke fixed-vector, short-latency saccadic eye movements with stimulation at low currents (Bruce and Goldberg, 1985; Moore and Fallah, 2001). U-Probes were then lowered for simultaneous measurements of visual LFP and spiking activity derived RFs at the same coordinates. After reaching the target depth we let the electrode settle for at least an hour before starting the recordings.

RF Measurements and Monkey Behavior

The visual probes to measure RFs consisted of white squares with an area of 1 dva^2 resulting in a positive luminance contrast of 60% (Michelson) and 3 (Weber) to the grey background (23.7 cd m^{-2}). The probe duration was less than 25 ms as measured with a photodiode.

In all three experimental conditions (Fixation 1, Fixation 2 and Presaccadic) the monkey was required to fixate one out of two fixation points (FP1 and FP2) placed 12 dva apart along the horizontal meridian. The fixation points FP1 and FP2 consisted of small (0.5 dva in diameter) red dots (23.6 cd m^{-2}). The saccade task consisted of a standard step task (Sommer and Wurtz, 2006) in which the fixation point (FP1) was displaced to a new location (FP2) and the monkey was rewarded for shifting its gaze to it. The fixation and presaccadic conditions differed in terms of the timing of the visual probe stimulus with respect to the saccade. In the two fixation conditions, the probe stimulus was presented at least 500 ms before a saccade. In the presaccadic condition, the probe presentation occurred while the monkey was still fixating at the location of FP1 but already planning a saccade to FP2. The monkey was rewarded with a drop of juice if he was still fixating at the required location at the end of the trial (>500 ms after probe presentation).

Fixation and saccade accuracy was excellent in both monkeys, with an average horizontal error of 0.01 dva (s.d. = 0.29) and an average vertical error of -0.02 dva (s.d. = 0.29) in fixation. The average saccade vector was 11.98 dva (s.d. = 0.52) with a horizontal landing error of -0.19 (s.d. = 0.35) and a vertical error of -0.05 dva (s.d. = 0.4). The average saccadic reaction time, that is, the time between target onset and saccade initiation, for monkey B was 229 ms (s.d. = 37) and 113 ms (s.d. = 35) for monkey N. For all reported analyses we used the responses to probes that were presented within a time window of 150 ms before saccade onset. Trials in which the probe was still on the screen when the saccade started, or was presented after the saccade, were excluded from the analyses. The average probe onset time was 82 ms before saccade onset (s.d. 38) for monkey B and 64 ms (s.d. 32) for monkey N; for further details see Zirnsak et al. (2014).

Power Spectral Density

Power spectral densities (PSDs) were calculated using Thomsons's multitaper method (e.g., Gregoriou et al., 2009; Jarvis and Mitra, 2001; Pesaran et al., 2008). Four orthogonal discrete prolate spheroidal (Slepian) sequences were used in the analysis. The frequency resolution of this method depends on the length of the signal. For example, for a 250 ms long LFP response, the frequency resolution is 4 Hz. On each trial, the baseline PSD was estimated using the LFPs during the period from (-350, -100] ms before probe onset. The baseline PSD was then subtracted from the stimulus or event related PSD. During fixation, we examined the periods from (0, 250] ms after probe onset. During the presaccadic period, we examined the time intervals from (0, 250] ms after probe onset, and (0, 250] ms, (125, 375] ms, (250, 500] ms, and (0, 500] ms after saccade onset.

Perpendicular Recordings and Current Source Density Analysis

We classified each linear array recording as either perpendicular or tangential based on the amount of RF displacement across array channels. Both LFP derived and spiking-derived RFs were used in the overall measure of the displacement. The displacement was measured as the systematic change in RF centers across channels and was computed via regression analyses on the RF centers. Recordings yielding significant regression coefficients were classified as tangential and recordings yielding non-significant

coefficients were classified as perpendicular (Figure 3A).

For the perpendicular recordings, we used current source density (CSD) analyses (Pettersen et al., 2006) to identify superficial, "granular", and deep layers of the FEF. The average LFP response during fixation across all probe locations was used for these analyses. Using only the RF center probe location yielded similar results, but was less reliable given the smaller number of trials. The CSD was calculated as the discrete double spatial derivative (Nicholson and Freeman, 1975) with "Vaknin" electrodes to yield the same number of CSD 'channels' as electrode channels (Vaknin et al., 1988). The CSD pattern was consistent across the 9 perpendicular penetrations and differed markedly from the tangential ones (Figure 3C). Within the perpendicular CSD pattern, the input ("granular") layer was defined as the compartment with a robust sink, which lay at a depth approximately corresponding to layer 4 of the FEF (0.7 – 1.0 mm). Superficial and deep layers, which had clearly different CSD, were defined as the compartments above and below the "granular layer".

REFERENCES

Britten, K.H., Shadlen, M.N., Newsome, W.T., and Movshon, J.A. (1993). Responses of neurons in macaque MT to stochastic motion signals. Vis Neurosci *10*, 1157-1169.

Bruce, C.J., and Goldberg, M.E. (1985). Primate frontal eye fields. I. Single neurons discharging before saccades. J Neurophysiol *53*, 603-635.

Gregoriou, G.G., Gotts, S.J., Zhou, H., and Desimone, R. (2009). High-frequency, long-range coupling between prefrontal and visual cortex during attention. Science *324*, 1207-1210.

Hikosaka, K., and Watanabe, M. (2000). Delay activity of orbital and lateral prefrontal neurons of the monkey varying with different rewards. Cereb Cortex *10*, 263-271.

Jarvis, M.R., and Mitra, P.P. (2001). Sampling properties of the spectrum and coherency of sequences of action potentials. Neural computation *13*, 717-749.

Moore, T., and Fallah, M. (2001). Control of eye movements and spatial attention. Proc Natl Acad Sci U S A *98*, 1273-1276.

Pesaran, B., Nelson, M.J., and Andersen, R.A. (2008). Free choice activates a decision circuit between frontal and parietal cortex. Nature *453*, 406-409.

Pettersen, K.H., Devor, A., Ulbert, I., Dale, A.M., and Einevoll, G.T. (2006). Current-source density estimation based on inversion of electrostatic forward solution: effects of finite extent of neuronal activity and conductivity discontinuities. J Neurosci Methods *154*, 116-133.

Vaknin, G., Discenna, P.G., and Teyler, T.J. (1988). A Method for Calculating Current Source Density (Csd) Analysis without Resorting to Recording Sites Outside the Sampling Volume. J Neurosci Meth *24*, 131-135.

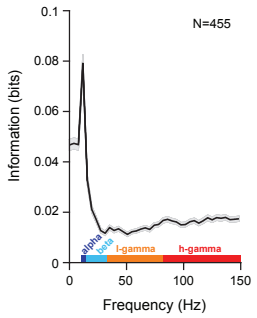

Figure S1. Mutual Information about Stimulus Location across LFP Frequencies, Related to Figure 1.

Mutual information was computed in discrete non-overlapping steps at 4 Hz resolutions. LFP frequency bands (alpha, beta, low-gamma, high-gamma) used for analyses are shown color-coded on top of the x-axis.

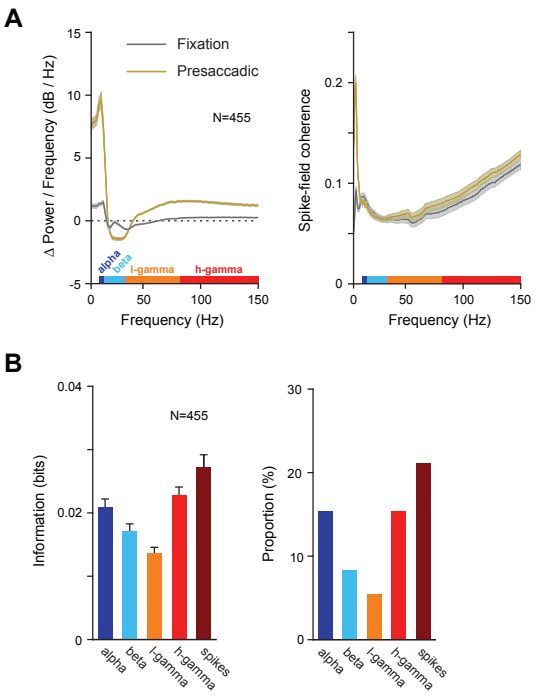

Figure S2. LFP Derived Visual Signals during Fixation and at the Time of Eye Movements, Related to Figure 1 & 5.

(A) Comparison of LFP power spectra and spike-field coherence. The left graph shows the LFP power spectra during fixation (gray) and at the time of saccades (gold). The shaded areas denote the standard error of the mean. The right graph shows the spike-field coherence during fixation (gray) and at the time of saccades (gold). Target LFP frequency bands used for analyses reported in the main text are shown color-coded on top of the x-axis of both graphs.

(B) Comparison of visual spatial information across different frequency bands. The left graph shows the average amount of mutual information about visual probe location contained within the LFP responses for a given frequency band and contained within the spiking activity, for the Presaccadic condition. Error bars denote the standard error of the mean. The right graph shows the percentage of recording sites across all experimental sessions, which yielded statistically significant mutual information for the different LFP frequency bands and the spiking activity. Although the LFP power and the spike-field coherence was generally higher during eye movement preparation for most frequencies as compared to fixation, the overall mutual information about the stimulus location and the number of recording sites yielding significant mutual information was lower.

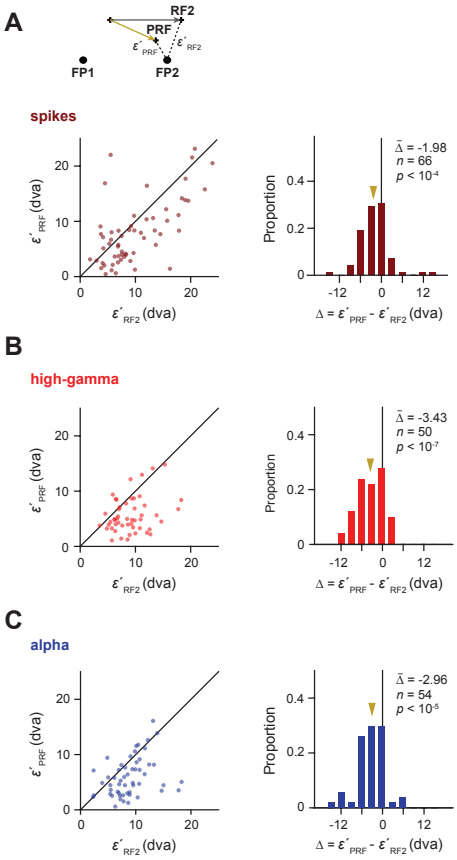

Figure S3. Comparison of Distances of the PRF and RF2 to FP2 ($\varepsilon'_{\mathrm{PRF}}$ $vs.$ $\varepsilon'_{\mathrm{RF2}}$) for all Significant Presaccadic RFs, Related to Figure 5.

(A) The graph shows $\varepsilon'_{\mathrm{PRF}}$ plotted against $\varepsilon'_{\mathrm{RF2}}$ for spiking RFs. PRFs were estimated from saccade aligned responses ((0-500] ms). The black line in the scatter plot denotes the line of unity. The gold vector in the histogram indicates the mean of the distribution.

(B) Comparison of $\varepsilon'_{\mathrm{PRF}}$ and $\varepsilon'_{\mathrm{RF2}}$ for high-gamma-band-derived RFs. Same conventions as in A.

(C) Comparison of $\varepsilon'_{\mathrm{PRF}}$ and $\varepsilon'_{\mathrm{RF2}}$ for alpha-band-derived RFs. Same conventions as in A. For all shown comparisons, PRFs are significantly closer to the saccade target than the RF2s.

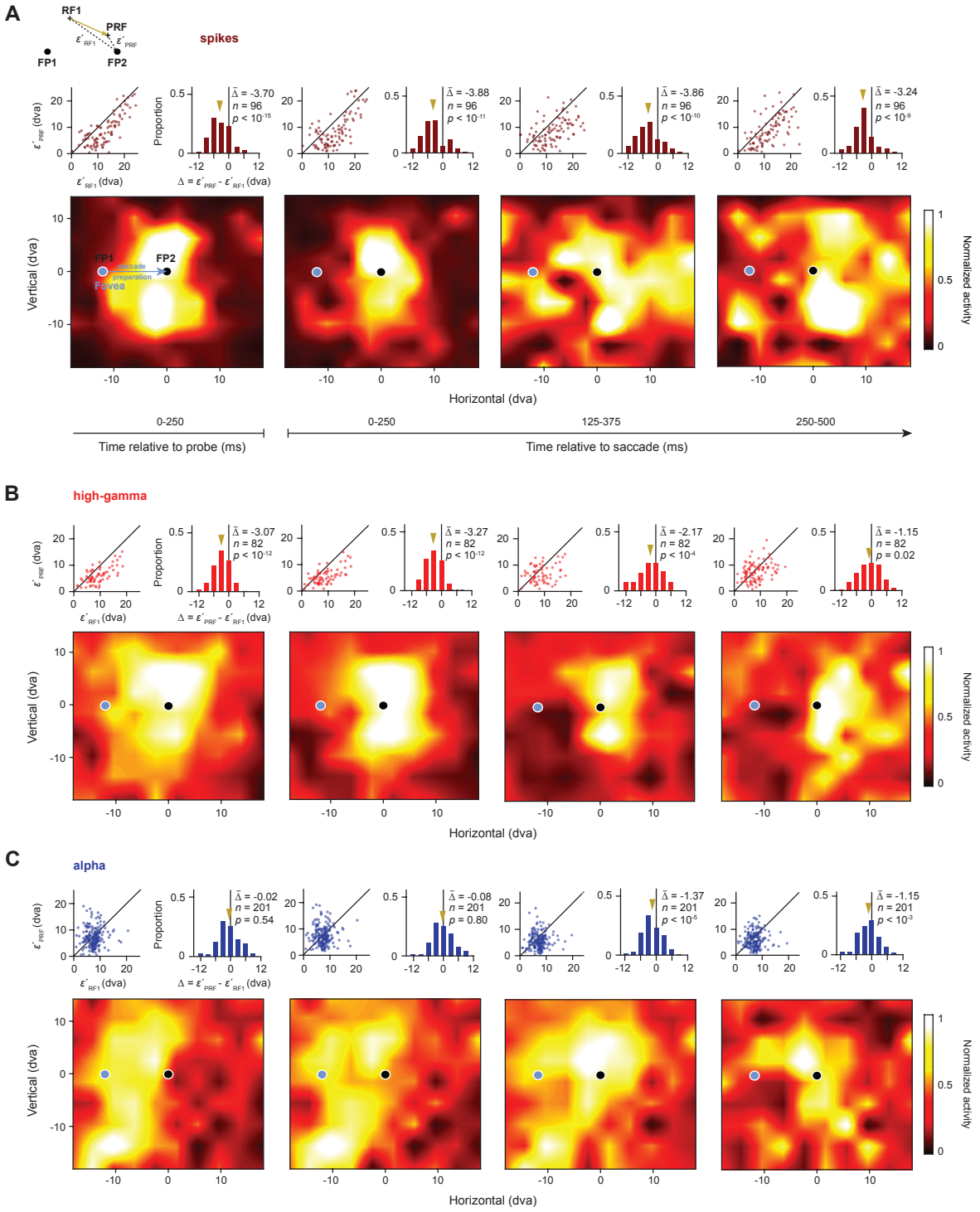

Figure S4. Dissociation of Alpha and High-gamma RFs at the Time of Eye Movements for all Significant Fixation RFs, Related to Figure 5.

(A) Population RFs derived from spiking activity to probes presented during saccade preparation from fixation point 1 (FP1) to fixation point 2 (FP2). Each map shows the population RF based on responses at different times relative to the eye movement. From left to right, Population RF aligned to probe onset (0-250] ms, Population RFs aligned to saccade onset (0-250] ms, (125-375] ms, and (250-500] ms. Bright areas indicate high levels of activity whereas dark areas depict low levels of activity. The insets on top of each population RF compare the distance $\varepsilon'_{\mathrm{PRF}}$ between the presaccadic RF centers (PRFs) and the saccade target (FP2) to the distance $\varepsilon'_{\mathrm{RF1}}$ between the fixation 1 RF centers (RF1s) and the FP2 for all significant fixation RFs (fixation 1 and fixation 2) (see Supplemental Experimental Procedures). Solid lines in the scatter plots depict the line of unity. Gold arrows in the histograms indicate the mean of the population.

(B) Population RFs derived from the high-gamma band. Same conversions as in A.

(C) Population RFs derived from the alpha band. Same conversions as in A. The population RFs have been spatially interpolated for visualization. In Figure 4, all population RFs and RF centers are based on, respectively from, statistically significant individual presaccadic RFs. Here we show the same results for recording sites with significant RFs during both Fixation 1 and Fixation 2 irrespective of their significance during the presaccadic epoch.

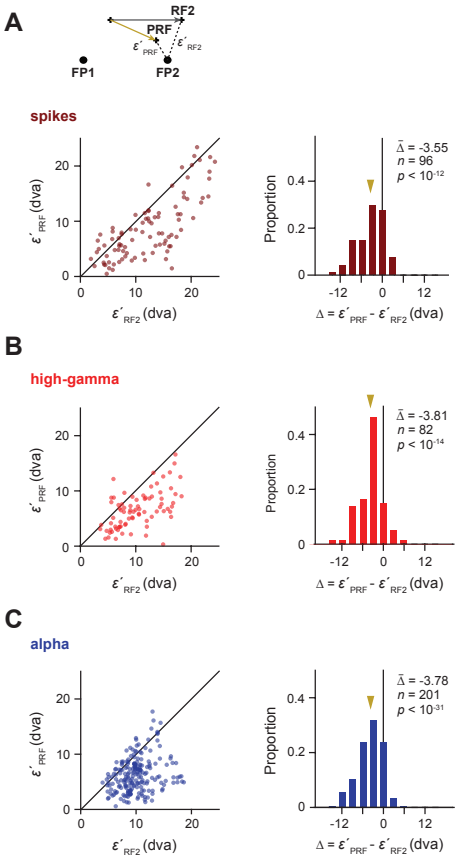

Figure S5. PRF to RF2 Comparison for all Significant Fxation RFs, Related to Figure 5.

(A) The graph shows $\varepsilon'_{\mathrm{PRF}}$ (distance between the PRF and FP2) plotted against $\varepsilon'_{\mathrm{RF2}}$ (distance between the RF2 and FP2) for spiking RFs. PRFs were estimated from saccade aligned responses ((0-500] ms). The black line in the scatter plot denotes the line of unity. The gold vector in the histogram indicates the mean of the distribution.

(B) Comparison of $\varepsilon'_{\mathrm{PRF}}$ and $\varepsilon'_{\mathrm{RF2}}$ for high-gamma-band-derived RFs. Same conventions as in A.

(C) Comparison of $\varepsilon'_{\mathrm{PRF}}$ and $\varepsilon'_{\mathrm{RF2}}$ for alpha-band-derived RFs. Same conventions as in A. For all shown comparisons, PRFs are significantly closer to the saccade target than the RF2s.

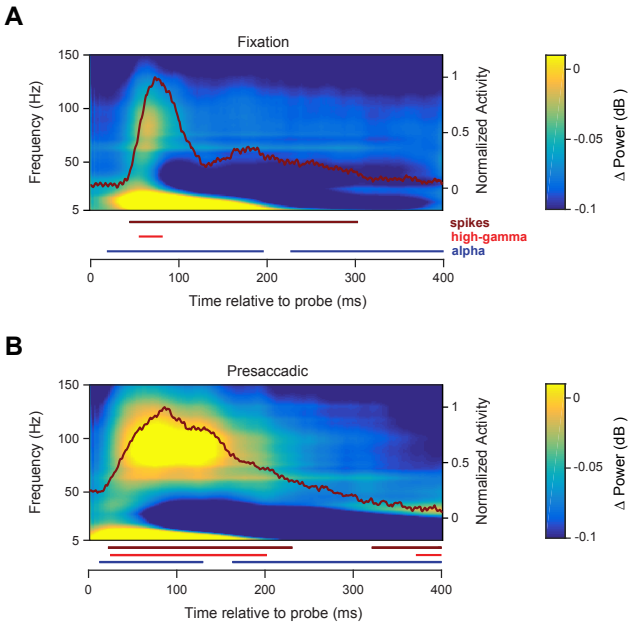

Figure S6. Average Time-frequency Power Spectra and Simultaneously Recorded Spiking Activities, Related to Figure 6.
(A) Average time-frequency spectrum and spiking activity across recordings and all stimulus locations relative to probe onset for the fixation conditions. Matching pursuit decomposition was used in calculating the spectrum to optimize temporal and frequency resolutions. An exponential kernel was used to estimate the average firing rate. Each spike therefore influences the estimate only forward in time. Lines below the graph indicate significant differences from baseline for the alpha band (blue), the high-gamma band (red), and the spiking activity (dark red).
(B) Average time-frequency spectrum and spiking activity relative across recordings and all stimulus locations to probe onset for the presaccadic condition. All the time-frequency spectra have been interpolated in both the frequency and temporal domain for visualization.

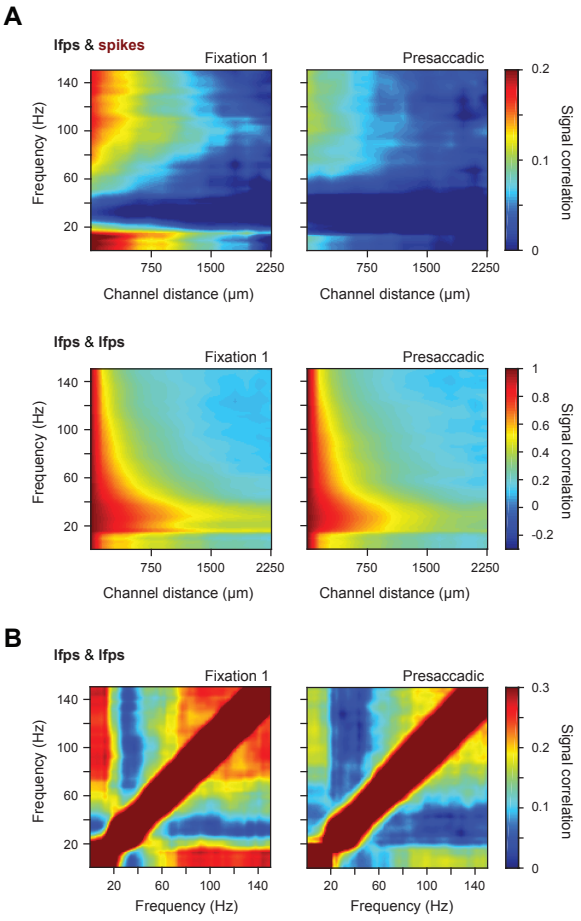

Figure S7. Comparison of Signal Correlations during Fixation and at the Time of Eye Movements, Related to Figure 6.

(A) Top, signal correlations between spiking responses to visual probes recorded at a reference channel (0 μm) and LFP responses recorded at distant channels of the linear electrode probe. Bottom, signal correlations between LFP responses recorded at a reference channel (0 μm) and LFP responses recorded at distant channels. The results has been spatially interpolated for visualization.

(B) Average signal correlation between different LFP frequencies recorded at the same electrode channels across all experimental sessions. Left, Fixation 1; right, Presaccadic. The results have been spatially interpolated for visualization